REAL-TIME 6DOF TERMINAL GUIDANCE FOR AUTONOMOUS SPACECRAFT CAPTURE FREE FLOATING OBJECTS USING STATE DEPENDENT MODEL PREDICTIVE CONTROL

Peng LI[(1)], Xiaokui YUE[(2)], Honghua DAI[(3)] , Xianbin CHI[(4)]
[(1)(2)(3) (4)]*National Key Laboratory of Aerospace Flight Dynamics, Northwestern Polytechnical University, Xi'an 710072, China,*
(1)+86 13991205708, SatLi@mail.nwpu.edu.cn
(2)+86 13571818923, xkyue@nwpu.edu.cn
(3)+86 15619393873, daihonghua@gmail.com
(4)+86 13629200134, stargazerxbc@hotmail.com

Abstract: *This paper investigates the optimal rendezvous with power-limited propulsion systems and collision avoidance. A 26-state dynamic model is established including both translational and rotational dynamics. This model is effective for describing autonomous rendezvous with both a three-axis attitude stabilized target and a tumbling one. Collisions are prevented through setting a safety sphere centered at the mass center of the target. Two rendezvous scenarios in actual missions are considered in this paper. The first case is to drive the chaser vehicle to rendezvous with a three-axis attitude stabilized target. A light-of-sight (LOS) tetrahedral path constraint is imposed for vision-based sensing and safety considerations. The second is to rendezvous with a tumbling target with an arbitrary docking port. The novel concept of tumbling plane is introduced to describe the tumbling motion. Then, the optimal-fuel rendezvous is transformed into a quadratic programming problem (QPP) using the state dependent model predictive control (SDMPC). Numerical simulations demonstrate that the proposed method can guarantee the safety of the autonomous rendezvous and to minimize the fuel consumption. In addition, this algorithm can be numerically solved rapidly.*

Keywords: *Optimal Rendezvous, Online trajectory planning, State Dependent Model Predictive Control.*

1. Introduction

Although significant development has been achieved in optimal rendezvous, rendezvous and capture a resident space object (RSO) still require human-in-the-loop operations. In contrast, Autonomous Rendezvous and Capture (ARC) require sensor suites that enable autonomous navigation and control with fault detection and recovery. Furthermore, ARC technology has also evolved with on-orbit service developments, such as the Demonstration for Autonomous Rendezvous Technology (DART), the Experimental Satellite Systems-11 (XSS-11) , and the Spacecraft for Universal Modification of Orbits (SUMO). These programs demonstrate that there is a need for an effective autonomous rendezvous optimal control algorithms which drive the chaser spacecraft rendezvous with the target under practical constraints.

Minimizing propellant consumption is critical to space operations, autonomous rendezvous to optimize fuel usage has been studied extensively [1]. In earlier study, few rendezvous problems were treated under realistic conditions, such

as limitation of thruster activation and collision avoidance. For example, Lembeck [2] investigate the low-thrust rendezvous in circular orbit without constraints. Guelman [3] investigate the optimal-fuel rendezvous in circular orbits with fixed terminal-approach direction. Due to the limitations in previous work, Richards et al. [4] introduced the MILP method for finding fuel-optimal trajectories subject to constraints of collision avoidance and prevention of thruster plumes. Based on Richards' research, Breger [5] studied online generation of safe, fuel-optimized trajectories that guarantee collision avoidance when system anomaly happens.

In recent years, David Benson [6] and Huntington [7] presented the Gauss pseudospectral method which is better at dealing with smoothing optimal problem, and it is receiving more attention in the field of optimal control. Boyarko [8] solved the problem of minimum-time and minimum-energy optimal rendezvous trajectories using both the Gauss pseudospectral approach and PMP. Unfortunately, since the optimal control problem is transformed into a NLP, it is difficult to get the solution of NLP in a short time especially when there are a large number of Gauss nodes. Lopez and Mclnnes [9] developed a novel guidance and control methodology that hinges on defining a suitable scalar function and that represents an artificial potential field describing the locality of the target vehicle. Mclnnes [10] and Ender [11] investigated the development and evaluation of potential function guidance for path constrained proximity maneuvers of spacecraft at the International Space Station. Epenoy [12] introduced an exacted penalty function to the solution of inequality state-constrained optimal control problems.

Although MPC has its origins in the process industries, it has recently been applied to trajectory planning problems because of some attractive characteristics. For example, MPC re-plans the optimal trajectory at each sampling instant and ARC typically has many constraints, including the limited thruster capability, collision avoidance and the dynamic characteristics of the target. Thus, Louis Breger [13] developed an online model predictive controller for spacecraft formation flying. Hartley [14] applied the MPC to provide trajectory guidance while Gavilan [15] presents a chance-constrained robust MPC for spacecraft rendezvous.

Due to fuel exhaust or ACS anomaly, it is common for the malfunctioned satellites to be spinning along a fixed axis as time goes on. Previous research work mainly focuses on a simplified case where the spinning axis is assumed to be parallel to or coincident with one of the orbital coordinate axes. Even though the space object is most likely to be tumbling along a fixed spinning axis, its axisymmetric axis for example, the fixed axis does not necessarily have to parallel to or coincide with one of the three axes in the orbital coordinate system. Accordingly, the current paper expands previous work by firstly introducing the novel concept of tumbling plane that is perpendicular to the spinning axis. For a tumbling object, the docking axis is constantly rotating within this plane. In this way, it would be convenient to describe the tumbling motion explicitly and mathematically for more general cases. Meanwhile, a safety sphere which centered at the target is constructed for the chaser spacecraft to avoid collision with the flexible appendages of the target.

To the best of the authors' knowledge, there has been no report on six degree-of-freedom control of spacecraft by applying the state dependent model predictive control (SDMPC). The current paper deals with the optimal-fuel rendezvous with an uncooperative space object. The basic objective is to drive the chaser vehicle with power-limited actuators under the conditions of path constraint and collision avoidance.

The structure of this paper is organized as follows. Section II presents a six DOF model to describe the relative motion, and gives the formulation of a rendezvous problem with path constraint and control magnitude limitation. The autonomous rendezvous problem considering docking port alignment and attitude maneuvering is formulated as a state dependent model predictive control (SDMPC) problem In Sec. III. Section IV presents simulation results and the effectiveness of the proposed method is discussed. Finally, the conclusions are given in Sec. V.

2. Rendezvous Modeling

2.1 Relative Translational Dynamics

The relative motion of the chaser with respect to the target is governed by the Hill–Clohessy–Wiltshire (HCW) equations. This model is expressed in the orbital frame which is centered at the target, OX points to the instantaneous velocity direction of the target, OZ is starts from the target to the center of the Earth, OY is mutually perpendicular to the OX and OZ axes, and $OX-OY-OZ$ forms a right-handed coordinate system. This frame can be illustrated in Fig. 1.

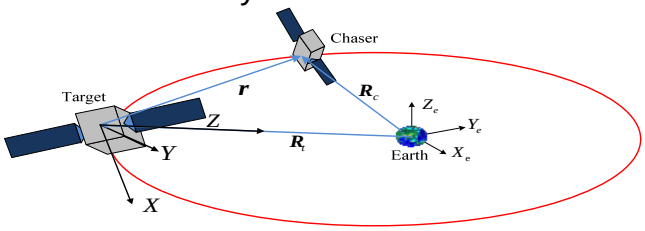

Figure 1. Spacecraft rendezvous geometry and coordinates

$$\begin{cases} \ddot{x}-2n\dot{z}=\dfrac{F_x}{m} \\ \ddot{y}+n^2y=\dfrac{F_y}{m} \\ \ddot{z}+2n\dot{x}-3n^2z=\dfrac{F_z}{m} \end{cases} \tag{1}$$

where m and n represent the mass and orbital angular velocity of the target, $\left(F_x,F_y,F_z\right)^{\mathrm{T}}$ denote the thruster forces expressed in the HCW frame. Define $\boldsymbol{r}$ as the relative states including the components of relative position and velocity, then the HCW equations can be written in the state-space representations

$$\dot{\boldsymbol{X}}^{\alpha}=\boldsymbol{A}^{\alpha}\boldsymbol{X}^{\alpha}+\boldsymbol{B}^{\alpha}\boldsymbol{U}^{\alpha} \tag{2}$$

where $\boldsymbol{X}^{\alpha}=\left(x,y,z,\dot{x},\dot{y},\dot{z}\right)^{\mathrm{T}}$ and $\boldsymbol{U}^{\alpha}=\left(u_x,u_y,u_z\right)^{\mathrm{T}}$ denotes the control acceleration, the state transition matrix $\boldsymbol{A}^{\alpha}$ and the control input matrix $\boldsymbol{B}^{\alpha}$ are given by

$$\boldsymbol{A}^{\alpha}=\begin{bmatrix}0&0&0&1&0&0\\0&0&0&0&1&0\\0&0&0&0&0&1\\0&0&0&0&0&2n\\0&-n^2&0&0&0&0\\0&0&3n^2&-2n&0&0\end{bmatrix},\qquad \boldsymbol{B}^{\alpha}=\begin{bmatrix}0&0&0\\0&0&0\\0&0&0\\1&0&0\\0&1&0\\0&0&1\end{bmatrix} \tag{3}$$

As can be seen, the radial z and along-track x components of the relative motion vector compose the in-plane motion which is uncoupled from the cross-track z component governed the out-of-plane motion. Although HCW equations are approximate formulations which ignored the influences of nonlinear factors when the target's orbit is elliptical, the HCW has widely been employed for rendezvous analysis. This is mainly because the autonomous rendezvous covers relatively short time spans. Consequently, HCW equations remain effective throughout our discussion in this paper.

In order to evaluate the states in the prediction horizon, the model is discretized with a sampling period T_s, yields a discrete-time model as:

$$\boldsymbol{X}_{k+1}^{\alpha}=\boldsymbol{A}_d^{\alpha}\boldsymbol{X}_k^{\alpha}+\boldsymbol{B}_d^{\alpha}\boldsymbol{U}_k^{\alpha} \tag{4}$$

where the states $\boldsymbol{X}_{k+1}^{\alpha}$ at the time instant $k+1$ can be computed by the states $\boldsymbol{X}_k^{\alpha}$ and control inputs $\boldsymbol{U}_k^{\alpha}$ at the time instant k, and the discrete state transition matrix $\boldsymbol{A}_d^{\alpha}$ and discrete input matrix $\boldsymbol{B}_d^{\alpha}$ for a single step can be expressed as

$$\boldsymbol{A}_d^{\alpha}=\begin{bmatrix}\boldsymbol{A}_{d11}&\boldsymbol{A}_{d12}&\boldsymbol{A}_{d13}&\boldsymbol{A}_{d14}&\boldsymbol{A}_{d15}&\boldsymbol{A}_{d16}\\\boldsymbol{A}_{d21}&\boldsymbol{A}_{d22}&\boldsymbol{A}_{d23}&\boldsymbol{A}_{d24}&\boldsymbol{A}_{d25}&\boldsymbol{A}_{d26}\\\boldsymbol{A}_{d31}&\boldsymbol{A}_{d32}&\boldsymbol{A}_{d33}&\boldsymbol{A}_{d34}&\boldsymbol{A}_{d35}&\boldsymbol{A}_{d36}\\\boldsymbol{A}_{d41}&\boldsymbol{A}_{d42}&\boldsymbol{A}_{d43}&\boldsymbol{A}_{d44}&\boldsymbol{A}_{d45}&\boldsymbol{A}_{d46}\\\boldsymbol{A}_{d51}&\boldsymbol{A}_{d52}&\boldsymbol{A}_{d53}&\boldsymbol{A}_{d54}&\boldsymbol{A}_{d55}&\boldsymbol{A}_{d56}\\\boldsymbol{A}_{d61}&\boldsymbol{A}_{d62}&\boldsymbol{A}_{d63}&\boldsymbol{A}_{d64}&\boldsymbol{A}_{d65}&\boldsymbol{A}_{d66}\end{bmatrix},\qquad \boldsymbol{B}_d^{\alpha}=\begin{bmatrix}\boldsymbol{B}_{d11}&\boldsymbol{B}_{d12}&\boldsymbol{B}_{d13}\\\boldsymbol{B}_{d21}&\boldsymbol{B}_{d22}&\boldsymbol{B}_{d23}\\\boldsymbol{B}_{d31}&\boldsymbol{B}_{d32}&\boldsymbol{B}_{d33}\\\boldsymbol{B}_{d41}&\boldsymbol{B}_{d42}&\boldsymbol{B}_{d43}\\\boldsymbol{B}_{d51}&\boldsymbol{B}_{d52}&\boldsymbol{B}_{d53}\\\boldsymbol{B}_{d61}&\boldsymbol{B}_{d62}&\boldsymbol{B}_{d63}\end{bmatrix} \tag{5}$$

Note that since $\boldsymbol{A}^{\alpha},\boldsymbol{B}^{\alpha}$ are constant matrices, thus, the discretized state transition matrix $\boldsymbol{A}_d^{\alpha}$ and input matrix $\boldsymbol{B}_d^{\alpha}$ are constant matrices either.

In order to describe the tumbling motion of the target, the tumbling frame $(OXYZ)_{tp}$ centered at the center of the target is established. The relationships between the tumbling frame and orbital frame can be seen in Fig. 2, the tumbling plane is constructed by $O_{tp}X_{tp}$ and $O_{tp}Z_{tp}$ axes with the rotating docking axis included. Specifically, $O_{tp}X_{tp}$, starting from the center of the target, points to the opposite direction of the velocity, $O_{tp}Z_{tp}$ is perpendicular to $O_{tp}X_{tp}$ along the direction of the angular velocity, and $O_{tp}X_{tp}-O_{tp}Y_{tp}-O_{tp}Z_{tp}$ forms a right-handed coordinate system.

Consequently, the scenario investigates autonomous rendezvous with a tumbling object. Define $\boldsymbol{\omega}^{tp}=\left(0,\omega,0\right)^{\mathrm{T}}$ as the angular velocity of the docking axis, and define $\boldsymbol{L}_k^{tp}=\left(L_x^{tp},L_y^{tp},L_z^{tp}\right)_k^{\mathrm{T}}$ as the docking axis vector expressed in the tumbling frame at the time instant k. As can be shown in Fig. 3, the docking axis vector coordinates $\boldsymbol{L}_{k+1}^{tp}$ at the time instant $k+1$ can be calculated by

$$\boldsymbol{L}_{k+1}^{tp}=\boldsymbol{R}\boldsymbol{L}_k^{tp} \tag{6}$$

$$\boldsymbol{R}=\begin{bmatrix}\cos(\omega T) & 0 & -\sin(\omega T)\\ 0 & 0 & 0\\ \sin(\omega T) & 0 & \cos(\omega T)\end{bmatrix} \tag{7}$$

where T represents the fixed time period. Please note that since $\omega = 0$ for the three-axis stabilized target, hence, $\boldsymbol{L}_{k+1}^{tp} = \boldsymbol{L}_{k}^{tp}$ for any time step.

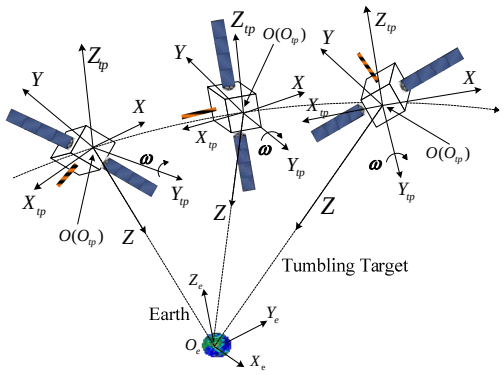

Figure 2. Relationships between the orbital frame and tumbling frame

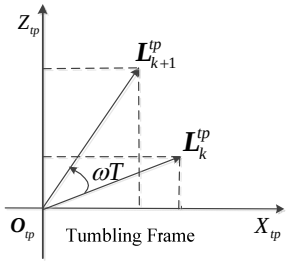

Figure 3. Docking axis coordinates in the tumbling frame

As shown in Fig. 4, define $\boldsymbol{\lambda}_k$ as the coordinates in the HCW frame from the docking port to the chaser at the time instant k. Since the relative state variables are defined in the orbit frame, therefore, the docking axis coordinates $\boldsymbol{L}^{tp}$ needs to be transformed into the HCW frame. Define $\boldsymbol{C}_{HCW}^{tp}$ as the rotation matrix from the tumbling frame to the HCW frame, and the matrix can be derived through two coordinate transformations. The relative position relationships between the mass centers of the two spacecraft and the docking port can be obtained by

$$\boldsymbol{\lambda}_k = \boldsymbol{r}_k - \boldsymbol{L}_k^{HCW} = \boldsymbol{r}_k - \boldsymbol{C}_{HCW}^{tp}\boldsymbol{L}_k^{tp} \tag{8}$$

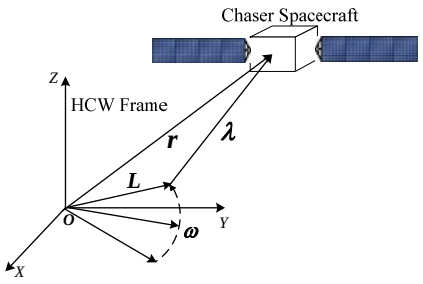

Figure 4. Relative position considering the length of the docking axis

Define the augmented state variables $\bar{\boldsymbol{X}}_k^{\alpha}$ in three-dimensional context as

$$\bar{\boldsymbol{X}}_k^{\alpha} = \left(\boldsymbol{r}_x, \boldsymbol{r}_y, \boldsymbol{r}_z, \dot{\boldsymbol{r}}_x, \dot{\boldsymbol{r}}_y, \dot{\boldsymbol{r}}_z, \boldsymbol{L}_x^{HCW}, \boldsymbol{L}_y^{HCW}, \boldsymbol{L}_z^{HCW}, \boldsymbol{\lambda}_x, \boldsymbol{\lambda}_y, \boldsymbol{\lambda}_z\right)^{\mathrm{T}} \tag{9}$$

Then, the whole model for describing the relative translation can be written as:

$$\bar{\boldsymbol{X}}_{k+1}^{\alpha} = \bar{\boldsymbol{A}}_d^{\alpha} \bar{\boldsymbol{X}}_k^{\alpha} + \bar{\boldsymbol{B}}_d^{\alpha} \bar{\boldsymbol{U}}_k \tag{10}$$

where

$$\bar{\boldsymbol{A}}_d^{\alpha} = \begin{bmatrix} \boldsymbol{A}_d^{\alpha}|_{6\times6} & \boldsymbol{0}_{6\times3} & \boldsymbol{0}_{6\times3} \\ \boldsymbol{0}_{3\times6} & \boldsymbol{R}_{3\times3} & \boldsymbol{0}_{3\times3} \\ [\boldsymbol{I}_{3\times3} \quad \boldsymbol{0}_{3\times3}] & -\boldsymbol{I}_{3\times3} & \boldsymbol{0}_{3\times3} \end{bmatrix} \qquad \bar{\boldsymbol{B}}_d^{\alpha} = \begin{bmatrix} \boldsymbol{B}_d^{\alpha}|_{6\times3} \\ \boldsymbol{0}_{6\times3} \end{bmatrix}$$

2.2 Safety Sphere Constructed for the Target

With consideration of the target's tumbling dynamic characteristics, it is possible for the chaser to collide with the flexible appendages equipped on the target. Hence, the safety sphere is constructed in order to avoid collision when approaching with a tumbling target. It is assumed that the angle between the orbital plane and tumbling plane is θ. The chaser is not allowed to enter this spherical region during the approaching process. In addition, the chaser needs to maneuver its attitude to match the angular velocity of the docking port.

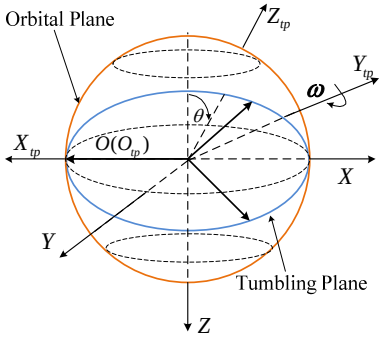

Figure 5. Transformation from the tumbling frame to the orbital frame

According to the definition of tumbling frame above, the rotation matrix $\boldsymbol{C}_{HCW}^{tp}$ can be derived through two coordinate transformations. As can be seen in Fig 5, first, the tumbling frame is rotated φ around the $O_{tp}Z_{tp}$ axis. Then, the new tumbling frame $(O'X'Y'Z')_{tp}$ is rotated ψ around the $O_{tp}^{'}X_{tp}^{'}$ axis. Consequently, the transformation matrix $\boldsymbol{C}_{HCW}^{tp}$ can be obtained by

$$\boldsymbol{C}_{HCW}^{tp} = \boldsymbol{C}_x(\psi) \cdot \boldsymbol{C}_z(\varphi) \tag{11}$$

where

$$\boldsymbol{C}_x(\psi) = \begin{bmatrix} 1 & 0 & 0 \\ 0 & \cos(\psi) & \sin(\psi) \\ 0 & -\sin(\psi) & \cos(\psi) \end{bmatrix} \qquad \boldsymbol{C}_z(\varphi) = \begin{bmatrix} \cos(\varphi) & \sin(\varphi) & 0 \\ -\sin(\varphi) & \cos(\varphi) & 0 \\ 0 & 0 & 1 \end{bmatrix} \tag{12}$$

In this paper, $\varphi = \pi$ and $\psi = \pi + \theta$. Define $\boldsymbol{C}_{HCW}^{I}$ as the rotation matrix from the inertial frame to the HCW frame. Hence, the rotation matrix from the inertial frame to the tumbling frame can be derived as

$$\boldsymbol{C}_{tp}^{I} = \boldsymbol{C}_{tp}^{HCW} \cdot \boldsymbol{C}_{HCW}^{I} \tag{13}$$

2.3 Euler Rotational Dynamics

Dynamics of the rotational motion of a rigid body (spacecraft) can be expressed by nonlinear continuous-time Euler's equations as

$$\boldsymbol{J}^{\Upsilon}\dot{\boldsymbol{\omega}}^{\Upsilon}+\boldsymbol{\omega}^{\Upsilon}\times\boldsymbol{J}^{\Upsilon}\boldsymbol{\omega}^{\Upsilon}=\boldsymbol{T}^{\Upsilon} \tag{14}$$

where $\Upsilon=\{C,T\}$ denote the chaser and target spacecraft respectively. The inertia matrix along the principal axes is $\boldsymbol{J}^{\Upsilon}=diag(\left[J_{11}^{\Upsilon},J_{22}^{\Upsilon},J_{33}^{\Upsilon}\right])$ where 'diag' represents a diagonal matrix. The angular velocity and control torque are presented as $\boldsymbol{\omega}^{\Upsilon}=\left[\omega_x^{\Upsilon},\omega_y^{\Upsilon},\omega_z^{\Upsilon}\right]^{\mathrm{T}}$ and $\boldsymbol{T}^{\Upsilon}=\left[T_x^{\Upsilon},T_y^{\Upsilon},T_z^{\Upsilon}\right]^{\mathrm{T}}$.

The attitude kinematics is governed by

$$\begin{bmatrix}\dot{q}_0^{\Upsilon}\\ \dot{q}_1^{\Upsilon}\\ \dot{q}_2^{\Upsilon}\\ \dot{q}_3^{\Upsilon}\end{bmatrix}=\frac{1}{2}\begin{bmatrix}-q_1^{\Upsilon}\omega_x^{\Upsilon}-q_2^{\Upsilon}\omega_y^{\Upsilon}-q_3^{\Upsilon}\omega_z^{\Upsilon}\\ q_0^{\Upsilon}\omega_x^{\Upsilon}+q_2^{\Upsilon}\omega_z^{\Upsilon}-q_3^{\Upsilon}\omega_y^{\Upsilon}\\ q_0^{\Upsilon}\omega_y^{\Upsilon}-q_1^{\Upsilon}\omega_z^{\Upsilon}+q_3^{\Upsilon}\omega_x^{\Upsilon}\\ q_0^{\Upsilon}\omega_z^{\Upsilon}+q_1^{\Upsilon}\omega_y^{\Upsilon}-q_2^{\Upsilon}\omega_x^{\Upsilon}\end{bmatrix} \tag{15}$$

The kinematic and dynamic models of spacecraft attitude are highly nonlinear equations which need to be transformed into a linear-like structure so that the rotational model can be written in a state-space form. Define $\boldsymbol{X}^{\Upsilon}=\left(q_0^{\Upsilon},q_1^{\Upsilon},q_2^{\Upsilon},q_3^{\Upsilon},\omega_x^{\Upsilon},\omega_y^{\Upsilon},\omega_z^{\Upsilon}\right)^{\mathrm{T}}$ as the state variables, Eqs. (14) and (15) can be synthesized as

$$\dot{\boldsymbol{X}}^{\Upsilon}=\boldsymbol{A}^{\Upsilon}(t)\boldsymbol{X}^{\Upsilon}+\boldsymbol{B}^{\Upsilon}\boldsymbol{U}^{\Upsilon} \tag{16}$$

$$\begin{bmatrix}\dot{q}_0^{\Upsilon}\\ \dot{q}_1^{\Upsilon}\\ \dot{q}_2^{\Upsilon}\\ \dot{q}_3^{\Upsilon}\\ \dot{\omega}_x^{\Upsilon}\\ \dot{\omega}_y^{\Upsilon}\\ \dot{\omega}_z^{\Upsilon}\end{bmatrix}=\frac{1}{2}\begin{bmatrix}0&-\omega_x^{\Upsilon}&-\omega_y^{\Upsilon}&-\omega_z^{\Upsilon}&0&0&0\\ \omega_x^{\Upsilon}&0&\omega_z^{\Upsilon}&-\omega_y^{\Upsilon}&0&0&0\\ \omega_y^{\Upsilon}&-\omega_z^{\Upsilon}&0&\omega_x^{\Upsilon}&0&0&0\\ \omega_z^{\Upsilon}&\omega_y^{\Upsilon}&-\omega_x^{\Upsilon}&0&0&0&0\\ 0&0&0&0&0&-2K_x^{\Upsilon}\omega_z^{\Upsilon}&0\\ 0&0&0&0&-2K_y^{\Upsilon}\omega_z^{\Upsilon}&0&0\\ 0&0&0&0&-2K_z^{\Upsilon}\omega_y^{\Upsilon}&0&0\end{bmatrix}\begin{bmatrix}q_0^{\Upsilon}\\ q_1^{\Upsilon}\\ q_2^{\Upsilon}\\ q_3^{\Upsilon}\\ \omega_x^{\Upsilon}\\ \omega_y^{\Upsilon}\\ \omega_z^{\Upsilon}\end{bmatrix}+\begin{bmatrix}0&0&0\\ 0&0&0\\ 0&0&0\\ 0&0&0\\ \frac{1}{J_{11}^{\Upsilon}}&0&0\\ 0&\frac{1}{J_{22}^{\Upsilon}}&0\\ 0&0&\frac{1}{J_{33}^{\Upsilon}}\end{bmatrix}\begin{bmatrix}T_x^{\Upsilon}\\ T_y^{\Upsilon}\\ T_z^{\Upsilon}\end{bmatrix} \tag{17}$$

Note that although the control input matrix $\boldsymbol{B}^{\Upsilon}$ is a constant matrix, the time dependent state variables $\omega_x^{\Upsilon},\omega_y^{\Upsilon},\omega_z^{\Upsilon}$ are incorporated in $\boldsymbol{A}^{\Upsilon}$, thus, $\boldsymbol{A}^{\Upsilon}$ is a state dependent coefficient matrix. Like the way the relative translational model is treated, the Euler rotational model also needs to be discretized. Define $\tilde{\boldsymbol{X}}_{k+1}^{\Upsilon}=\left(q_0^{\Upsilon},q_1^{\Upsilon},q_2^{\Upsilon},q_3^{\Upsilon},\omega_x^{\Upsilon},\omega_y^{\Upsilon},\omega_z^{\Upsilon}\right)_{k+1}^{\mathrm{T}}$ as the state variables at the time instant $k+1$, the discretized attitude model can be written as

$$\tilde{\boldsymbol{X}}_{k+1}^{\Upsilon}=\tilde{\boldsymbol{A}}_k^{\Upsilon}\tilde{\boldsymbol{X}}_k^{\Upsilon}+\tilde{\boldsymbol{B}}_k^{\Upsilon}\tilde{\boldsymbol{U}}_k^{\Upsilon} \tag{18}$$

where $\tilde{\boldsymbol{U}}_k^{\Upsilon}=\left(T_x^{\Upsilon},T_y^{\Upsilon},T_z^{\Upsilon}\right)_k^{\mathrm{T}}$ denotes the control torque at the time instant k. Please note that unlike $\boldsymbol{A}_d^{\alpha},\boldsymbol{B}_d^{\alpha}$ which are constant matrices at any step, discretized state transition matrix $\tilde{\boldsymbol{A}}_k^{\Upsilon}$ and input matrix $\tilde{\boldsymbol{B}}_k^{\Upsilon}$ are time-varying at every time step. This is because $\boldsymbol{A}^{\Upsilon}$ is a state dependent coefficient matrix including angular velocity components.

2.4 6DOF Dynamic Model

Based on Eqs. (10) and (18), define $\boldsymbol{X}_k = \left(\bar{\boldsymbol{X}}_k^{\alpha}, \tilde{\boldsymbol{X}}_k^{C}, \tilde{\boldsymbol{X}}_k^{T} \right)$, then a 26-state dynamic model governing rendezvous dynamics can be given as

$$\boldsymbol{X}_{k+1} = \boldsymbol{A}_k \boldsymbol{X}_k + \boldsymbol{B}_k \boldsymbol{U}_k \tag{19}$$

where

$$\boldsymbol{A}_{26\times 26} = \begin{bmatrix} \bar{\boldsymbol{A}}_d^{\alpha}\,|_{12\times 12} & & \\ & \tilde{\boldsymbol{A}}_k^{C}\,|_{7\times 7} & \\ & & \tilde{\boldsymbol{A}}_k^{T}\,|_{7\times 7} \end{bmatrix} \qquad \boldsymbol{B}_{26\times 9} = \begin{bmatrix} \bar{\boldsymbol{B}}_d^{\alpha}\,|_{12\times 3} & & \\ & \tilde{\boldsymbol{B}}_k^{C}\,|_{7\times 3} & \\ & & \tilde{\boldsymbol{B}}_k^{T}\,|_{7\times 3} \end{bmatrix}$$

This dynamic model will be used as recursive equations for predicting system states in future steps. The procedure will be outlined in the following section.

3 SDMPC Formulation for Optimal Rendezvous

3.1 State Dependent Model Predictive Control Formulation

In this section, the SDMPC optimization technique is proposed to address the class of nonlinear time-varying systems described by Eq. (19), and the procedure of transforming the optimal rendezvous into a QPP is formulated.

3.1.1 Prediction of the Control Inputs

As is shown above, the state variables $\boldsymbol{X}_{k+i}, i = 1, 2, ..., N$ at future steps can be obtained by repeatedly using the recursive equations based on the initial values $\boldsymbol{X}_k$ and $\boldsymbol{U}_k$. Define $\boldsymbol{U}_{k-1}$ and $\Delta\boldsymbol{U}_k$ as the control inputs for the step $k-1$ and the control correction variables for the step k, accordingly the control inputs at step k can be computed by

$$\boldsymbol{U}_k = \boldsymbol{U}_{k-1} + \Delta\boldsymbol{U}_k \tag{20}$$

Then the SPM Eq. (19) can be transformed into the following form

$$\begin{bmatrix} \boldsymbol{X}_{k+1} \\ \boldsymbol{U}_k \end{bmatrix} = \begin{bmatrix} \boldsymbol{A}_k & \boldsymbol{B}_k \\ \boldsymbol{0} & \boldsymbol{I} \end{bmatrix} \begin{bmatrix} \boldsymbol{X}_k \\ \boldsymbol{U}_{k-1} \end{bmatrix} + \begin{bmatrix} \boldsymbol{B}_k \\ \boldsymbol{I} \end{bmatrix} \Delta\boldsymbol{U}_k \tag{21}$$

Please note that the iterative equations above are based on the determined inputs, so that the iterative computations can proceed. Define N and N_c as the prediction horizon and the control horizon variable respectively. It is assumed that $\Delta\boldsymbol{U}(k+i\,|\,k), i = 0, ..., (N_c - 1)$ is the control correction variables calculated from the time instant k forwards. During the SDMPC derivation, $\Delta\boldsymbol{U}(k+i\,|\,k), i = 0, ..., (N_c - 1)$ are obtained as the results of solving the QPP numerically.

Accordingly, the control variables $\boldsymbol{U}(k+i\,|\,k), i = 0, ..., (N_c - 1)$ over the next N_c steps can be obtained by using the control correction variables. The control prediction model (CPM) in the prediction horizon is given by

$$\boldsymbol{U}(k+i\,|\,k) = \sum_{i=0}^{N_c-1} \Delta\boldsymbol{U}(k+i\,|\,k) + \boldsymbol{U}(k-1) \tag{22}$$

Assuming $\boldsymbol{U}_c(k)$ and $\Delta\boldsymbol{U}_c(k)$ as the column vectors including the predicted control inputs and control correction variables respectively in which the parameter k denotes that these values are computed from the time instant k forwards. The expressions can be given by

$$\boldsymbol{U}_c(k)=\begin{bmatrix}\boldsymbol{U}(k\,|\,k)\\ \vdots \\ \boldsymbol{U}(k+N_c-1\,|\,k)\end{bmatrix} \qquad \Delta\boldsymbol{U}_c(k)=\begin{bmatrix}\Delta\boldsymbol{U}(k\,|\,k)\\ \vdots \\ \Delta\boldsymbol{U}(k+N_c-1\,|\,k)\end{bmatrix} \tag{23}$$

3.1.2 Prediction of the States

Based on the recursive Eq. (19) and the CPM Eq. (22), the system states expressed by the predicted control inputs $\boldsymbol{U}(k+i\,|\,k),\ i=0,...,(N_c-1)$ could be computed by

$$\boldsymbol{X}(k+j\,|\,k)=\boldsymbol{A}^j\boldsymbol{X}(k)+\begin{bmatrix}\boldsymbol{A}^{j-1} & \boldsymbol{A}^{j-2} & \dots & \boldsymbol{I}\end{bmatrix}\boldsymbol{B}\boldsymbol{U}_c(k) \tag{24}$$

Assuming $\boldsymbol{X}_c^{\,p}(k)$ and $\boldsymbol{X}_c^{\,ref}(k)$ as the column vectors including predictive states and reference states respectively in which the parameter k denotes that these values are computed from the time instant k forwards. The expressions can be given by

$$\boldsymbol{X}_c^{\,p}(k)=\begin{bmatrix}\boldsymbol{X}(k+1\,|\,k)\\ \vdots \\ \boldsymbol{X}(k+N\,|\,k)\end{bmatrix} \qquad \boldsymbol{X}_c^{\,ref}(k)=\begin{bmatrix}\boldsymbol{X}_{ref}(k+1\,|\,k)\\ \vdots \\ \boldsymbol{X}_{ref}(k+N\,|\,k)\end{bmatrix} \tag{25}$$

Although the states can be obtained using the predicted control column vector $\boldsymbol{U}_c(k)$, the states recursive equations need to be transformed. This is primarily because the control correction variables are the direct results by solving the optimization problem, hence, the states recursive equations need to be transformed and expressed by $\Delta\boldsymbol{U}_c(k)$. However, due to $N\geq N_c$, it is assumed that $\Delta\boldsymbol{U}(k+i\,|\,k)=0$ when $N_c\leq i\leq(N-1)$. In other words, the predicted control variables $\boldsymbol{U}(k+i\,|\,k)$ in the horizon $N_c\leq i\leq(N-1)$ equal to the last predicted control variables in the prediction horizon $\boldsymbol{U}(k+N_c-1\,|\,k)$.

For the case $1\leq j\leq N_c$, the states recursive equations expressed by the control correction column vector are given by

$$\boldsymbol{X}(k+j\,|\,k)=\boldsymbol{A}^j\boldsymbol{X}(k)+\left[\sum_{m=0}^{N_c-1}\boldsymbol{A}^m\boldsymbol{B}\dots\boldsymbol{B}\right]\Delta\boldsymbol{U}_c(k)+\left(\sum_{m=0}^{j-1}\boldsymbol{A}^m\right)\boldsymbol{B}\boldsymbol{U}(k-1) \tag{26}$$

For the case $(N_c+1)\leq j\leq N$, the states recursive equations are given by

$$\boldsymbol{X}(k+j\,|\,k)=\boldsymbol{A}^j\boldsymbol{X}(k)+\left[\sum_{m=0}^{N_c-1}\boldsymbol{A}^m\boldsymbol{B}\dots\boldsymbol{B}\right]\Delta\boldsymbol{U}_c(k)+\sum_{m=0}^{N-N_c}\boldsymbol{A}^m\boldsymbol{B}\Delta\boldsymbol{U}(k+N_c-1\,|\,k)+\left(\sum_{m=0}^{j-1}\boldsymbol{A}^m\right)\boldsymbol{B}\boldsymbol{U}(k-1) \tag{27}$$

Finally, by integrating Eqs. (26) and (27), the state prediction model (SPM) expressed by the control correction column vector $\Delta\boldsymbol{U}_c(k)$ in the prediction horizon N can be written as

$$\boldsymbol{X}_c^{\,p}(k)=\boldsymbol{\phi}\boldsymbol{X}(k)+\boldsymbol{\Gamma}\boldsymbol{U}(k-1)+\boldsymbol{G}_y\Delta\boldsymbol{U}_c(k) \tag{28}$$

where $\boldsymbol{X}_c^{\,p}(k)$ is a state column vector and $\boldsymbol{\phi}=\boldsymbol{A}^j,\ \boldsymbol{\Gamma}=\sum_{i=0}^{j-1}\boldsymbol{A}^i\boldsymbol{B},\ \boldsymbol{G}_y=\begin{bmatrix}\sum_{i=0}^{j-1}\boldsymbol{A}^i\boldsymbol{B} & \cdots & \sum_{i=0}^{j-N_c}\boldsymbol{A}^i\boldsymbol{B}\end{bmatrix}$.

$$\begin{bmatrix} \boldsymbol{X}(k+1|k) \\ \vdots \\ \boldsymbol{X}(k+N_c|k) \\ \boldsymbol{X}(k+N_c+1|k) \\ \vdots \\ \boldsymbol{X}(k+N|k) \end{bmatrix} = \underbrace{\begin{bmatrix} \boldsymbol{A} \\ \vdots \\ \boldsymbol{A}^{N_c} \\ \boldsymbol{A}^{N_c+1} \\ \vdots \\ \boldsymbol{A}^{N} \end{bmatrix}}_{\boldsymbol{\phi}} \boldsymbol{X}(k) + \underbrace{\begin{bmatrix} \boldsymbol{B} \\ \vdots \\ \sum_{i=0}^{N_c-1} \boldsymbol{A}^i\boldsymbol{B} \\ \sum_{i=0}^{N_c} \boldsymbol{A}^i\boldsymbol{B} \\ \vdots \\ \sum_{i=0}^{N-1} \boldsymbol{A}^i\boldsymbol{B} \end{bmatrix}}_{\boldsymbol{\Gamma}} \boldsymbol{U}(k-1) + \underbrace{\begin{bmatrix} \boldsymbol{B} & \cdots & \boldsymbol{0} \\ \boldsymbol{AB}+\boldsymbol{B} & \cdots & \boldsymbol{0} \\ \vdots & \ddots & \vdots \\ \sum_{i=0}^{N_c-1} \boldsymbol{A}^i\boldsymbol{B} & \cdots & \boldsymbol{B} \\ \sum_{i=0}^{N_c} \boldsymbol{A}^i\boldsymbol{B} & \cdots & \boldsymbol{AB}+\boldsymbol{B} \\ \vdots & \vdots & \vdots \\ \sum_{i=0}^{N-1} \boldsymbol{A}^i\boldsymbol{B} & \cdots & \sum_{i=0}^{N-N_c} \boldsymbol{A}^i\boldsymbol{B} \end{bmatrix}}_{\boldsymbol{G}_y} \begin{bmatrix} \Delta\boldsymbol{U}(k|k) \\ \vdots \\ \Delta\boldsymbol{U}(k+N_c-1|k) \end{bmatrix} \tag{29}$$

3.1.3 Cost Function

The cost function for the SDMPC is designed to penalize the error between the predictive states and the reference states in the predictive horizon, while to minimize the fuel consumption in the control horizon. The cost function at the time instant k is given by:

$$J_k = \sum_{j=1}^{N} \left\| \boldsymbol{X}(k+j|k) - \boldsymbol{X}_{ref}(k+j|k) \right\|_{\boldsymbol{Q}}^2 + \sum_{i=0}^{N_c-1} \left\| \Delta\boldsymbol{U}(k+i|k) \right\|_{\boldsymbol{R}}^2 \tag{30}$$

where $\boldsymbol{Q}$ is the state weighing matrix, $\boldsymbol{R}$ is the control weighting matrix, and $\boldsymbol{X}_{ref}(k+j|k), j=1,...,N$ is the reference trajectory of the state variables calculated at the time instant k. In order to ensure $J_k \geq 0$, $\boldsymbol{Q}$ is assumed to be a positive semi-definite constant matrix and $\boldsymbol{R}$ is assumed to be a positive-definite constant matrix. Note that the weighting matrices $\boldsymbol{Q}$ and $\boldsymbol{R}$ are closely related to the properties of the control results, and therefore need to be tuned in the numerical simulation to obtain a satisfactory performance.

3.1.4 Transform the Optimal Rendezvous into QPP

Then, the cost function (30) can be rewritten as

$$J_k = \left\| \boldsymbol{X}_c^p(k) - \boldsymbol{X}_c^{ref}(k) \right\|_{\boldsymbol{Q}}^2 + \left\| \Delta\boldsymbol{U}_c(k) \right\|_{\boldsymbol{R}}^2 \tag{31}$$

Define $\boldsymbol{E}$ as the auxiliary variables, and $\boldsymbol{E}(k)$ calculated at the time instant k can be obtained by

$$\boldsymbol{E}(k) = \boldsymbol{X}_c^{ref}(k) - \boldsymbol{\phi}\boldsymbol{X}(k) - \boldsymbol{\Gamma}\boldsymbol{U}(k-1) \tag{32}$$

Note that $\boldsymbol{E}(k)$ is a $N_c \times 1$ column vector and can be calculated as a constant vector at the time instant k. Transform the cost function into the following form by inserting (32) into (31)

$$\begin{aligned} J_k &= \left\| \boldsymbol{G}_y \Delta\boldsymbol{U}_c(k) - \boldsymbol{E}(k) \right\|_{\boldsymbol{Q}}^2 + \left\| \Delta\boldsymbol{U}_c(k) \right\|_{\boldsymbol{R}}^2 \\ &= \left[\Delta\boldsymbol{U}_c(k)\boldsymbol{G}_y^{\mathrm{T}} - \boldsymbol{E}^{\mathrm{T}}(k) \right] \boldsymbol{Q} \left[\boldsymbol{G}_y \Delta\boldsymbol{U}_c(k) - \boldsymbol{E}(k) \right] + \Delta\boldsymbol{U}_c^{\mathrm{T}}(k)\boldsymbol{R}\Delta\boldsymbol{U}_c(k) \\ &= \Delta\boldsymbol{U}_c^{\mathrm{T}}(k) \left[\boldsymbol{G}_y^{\mathrm{T}}\boldsymbol{Q}\boldsymbol{G}_y + \boldsymbol{R} \right] \Delta\boldsymbol{U}_c(k) - 2\boldsymbol{E}^{\mathrm{T}}(k)\boldsymbol{Q}\boldsymbol{G}_y\Delta\boldsymbol{U}_c^{\mathrm{T}}(k) + \boldsymbol{E}^{\mathrm{T}}(k)\boldsymbol{Q}\boldsymbol{E}(k) \end{aligned} \tag{33}$$

Finally, the cost function can be simplified into the following form

$$J_k = \frac{1}{2}\Delta\boldsymbol{U}_c^{\mathrm{T}}(k)\boldsymbol{H}\Delta\boldsymbol{U}_c(k) + \boldsymbol{f}^{\mathrm{T}}\Delta\boldsymbol{U}_c(k) + const \tag{34}$$

where $\boldsymbol{H} = 2(\boldsymbol{G}_y^{\mathrm{T}}\boldsymbol{Q}\boldsymbol{G}_y + \boldsymbol{R})$, $\boldsymbol{f} = -2\boldsymbol{G}_y^{\mathrm{T}}\boldsymbol{Q}\boldsymbol{E}(k)$. As shown, the optimal rendezvous has been transformed into a standard QPP, and the solution of the QPP can be solved by using the Matlab in a fast manner.

3.2. Constraints On the problem

A series of practical control constraints that might be imposed in actual missions are considered. Therefore, the control inputs at any step should be sought to minimize the cost function over the prediction horizon while satisfying these constraints at the same time.

3.2.1 Collision Avoidance through Tetrahedral Path Constraint

Unlike previous research work, the light-of-sight (LOS) tetrahedral cone established here is assumed to protrude from the docking port, not the mass center of the target. The chaser spacecraft is required to remain within this region during the approaching process for relative position and attitude measurements by using vision-based navigation system. As is shown in Fig. 6, the tetrahedral region can be described mathematically as

$$\begin{cases} -\tan\alpha \le \dfrac{\boldsymbol{r}_z}{\boldsymbol{r}_x + l} \le \tan\alpha \\ -\tan\beta \le \dfrac{\boldsymbol{r}_y}{\boldsymbol{r}_x + l} \le \tan\beta \end{cases} \tag{35}$$

where α and β are the half cone angles along the z axis and the y axis respectively. Further, the inequalities above can be rewritten as

$$\begin{cases} (\boldsymbol{r}_x + l)\tan\alpha + \boldsymbol{r}_z \le 0, (\boldsymbol{r}_x + l)\tan\alpha - \boldsymbol{r}_z \le 0 \\ (\boldsymbol{r}_x + l)\tan\beta + \boldsymbol{r}_y \le 0, (\boldsymbol{r}_x + l)\tan\beta - \boldsymbol{r}_y \le 0 \end{cases} \tag{36}$$

Finally, the LOS constraint equations are formulated as

$$\boldsymbol{A}_s \cdot \boldsymbol{X}_k^{\alpha} \le -\boldsymbol{L} \tag{37}$$

where

$$\boldsymbol{A}_s = \begin{bmatrix} 1 & 0 & \dfrac{1}{\tan\alpha} & 0 & 0 & 0 \\ 1 & 0 & \dfrac{-1}{\tan\alpha} & 0 & 0 & 0 \\ 1 & \dfrac{-1}{\tan\beta} & 0 & 0 & 0 & 0 \\ 1 & \dfrac{1}{\tan\beta} & 0 & 0 & 0 & 0 \end{bmatrix} \qquad \boldsymbol{L} = -\begin{bmatrix} l \\ l \\ l \\ l \end{bmatrix} \tag{38}$$

Expand $\boldsymbol{A}_s, \boldsymbol{L}$ into $\bar{\boldsymbol{A}}_s = [\boldsymbol{A}_s, \boldsymbol{0}_{4\times 20}]$ and $\bar{\boldsymbol{L}} = [\boldsymbol{L}^{\mathrm{T}}, \boldsymbol{0}_{1\times 20}]^{\mathrm{T}}$ to include the other state variables. Then, insert Eq. (37) into the state prediction model Eq. (19), then the inequality constraints become

$$\bar{\boldsymbol{A}}_s\boldsymbol{G}_y\Delta\boldsymbol{U}_c(k) \le \bar{\boldsymbol{L}} - \bar{\boldsymbol{A}}_s\boldsymbol{\phi}\boldsymbol{X}_c^{p}(k) - \bar{\boldsymbol{A}}_s\boldsymbol{\Gamma}\boldsymbol{U}(k-1) \tag{39}$$

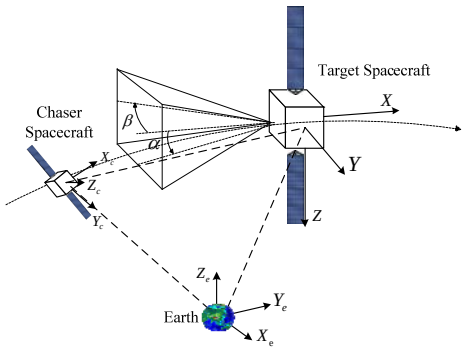

Figure 6. LOS Region Protrudes From the Docking Port of the Target

3.2 Receding Horizon Optimization Strategy

In this paper, the orbit and attitude maneuvering trajectory for the chaser spacecraft is composed of a sequence of locally optimal segments. At a certain time step, the reference states $\boldsymbol{X}_c^{ref}(k)$ will be predicted for the N future time steps based on the initial values. By solving the QPP, the control correction variables $\Delta \boldsymbol{U}_c(k)$ are obtained, which could be used to predict the control inputs over the next N_c steps. However, only a subset of these control input commands are actually implemented. Usually the applied subset is restricted to the first control input. Then, the extracted first control input is used to compute the new system states based on the SPM. Both the control input and new system states will be used as initial values for the next cycle.

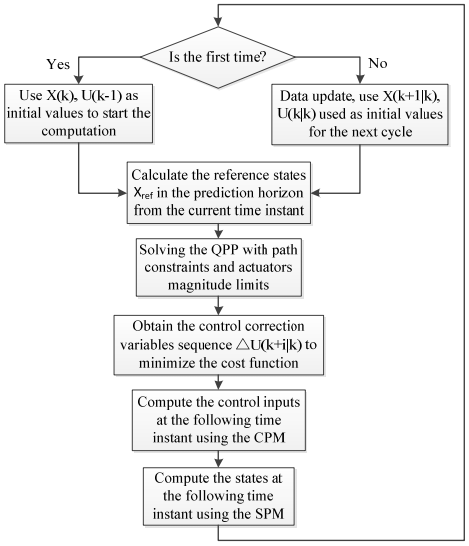

Figure 7. Flow diagram of the receding horizon optimization strategy

4 Numerical Examples

In this section, two rendezvous scenarios are given to show the validity and advantages of the proposed method. The simulations are conducted on a computer with a 2.0GHz dual-core CPU and 2.00 GB RAM by using Matlab.

4.1 Three-axis Attitude Stabilized Target

The docking direction is assumed to point to the opposite direction of the target's velocity. Hence, the chaser needs to rendezvous with the target along the V-bar direction. However, the LOS tetrahedral path constraint applied here is also suitable for approaching from the R-Bar and H-Bar direction. Please note that unlike most of the previous research, the start point of the chaser does not lie in the light-of-sight region and its extension. The objective of the control is to drive the chaser spacecraft approach the target along the fixed docking direction while to meet the light-of-sight constraint.

The height of the target satellite is $800km$, the orbital rate is $n = 0.001rad/s$, and the total maneuver simulation time is 40 seconds. Through multiple simulations, the control horizon and prediction horizon are $N_c = 20$ and $N = 55$ respectively. The weighting matrices are chosen to be: $\boldsymbol{Q} = 0.01 \times I_{N \cdot state\_num}$, $\boldsymbol{R} = 50 \times I_{N_c \cdot ctrl\_num}$. The angles which determine the size of the tetrahedral cone are $\alpha = 30^\circ$, $\beta = 30^\circ$ and the docking axis is assumed to be 3 meters long. The target and chaser spacecraft masses are 800.0 Kg and 400.0 Kg respectively.

Table 1. Initial values for the five chaser satellites

No.	position(m)	velocity(m/s)	Quaternions	Ang.V (rad/s)
Sat 1	[-40, 5, -25]	[0.5, 1, 3.5]	[0.8602,0.1, 0.3, 0.4]	[-0.01, 0.05, 0.07]
Sat 2	[-40, 20, 10]	[0.5, -4, -0.5]	[0.5, -0.5, 0.5, -0.5]	[-0.02, 0.03, -0.09]
Sat 3	[-40, 3, -5]	[0.5, -3, 3]	[0.1,0.4,0.5831,0.7]	[0.06, -0.02, -0.03]
Sat 4	[-40, -20, -15]	[0.5, 3, -0.5]	[-0.2,0.3,-0.5,0.7874]	[-0.02, 0.08, -0.05]
Sat 5	[-40, -5, 20]	[0.5, -0.4, -5]	[0.2,0.3, 0.4, 0.8426]	[0.05, -0.01, -0.03]

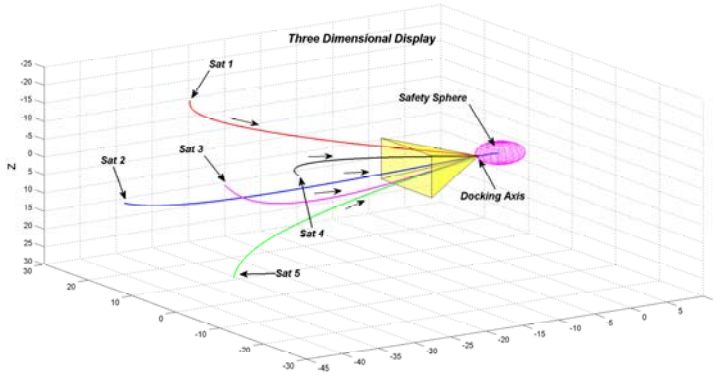

Figure 8. Approaching a stationary target seen at the back of the target

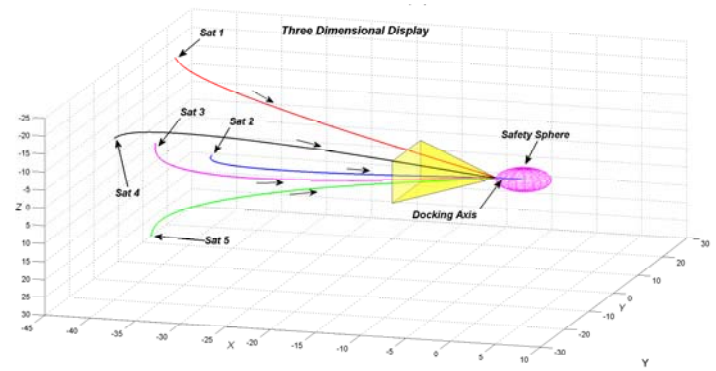

Figure 9. Approaching a stationary target seen at the front of the target

Figs.8 and 9 illustrate the optimized approaching trajectory from the V-bar direction with safety constraints satisfied. While Figs. 10 to 14 show the relative motion states time histories of five chaser satellites. As could be seen above, the spacecraft is driven to approach the target along V-bar direction while satisfying the LOS constraint and the chaser finally enter into the LOS region which achieves a successful docking.

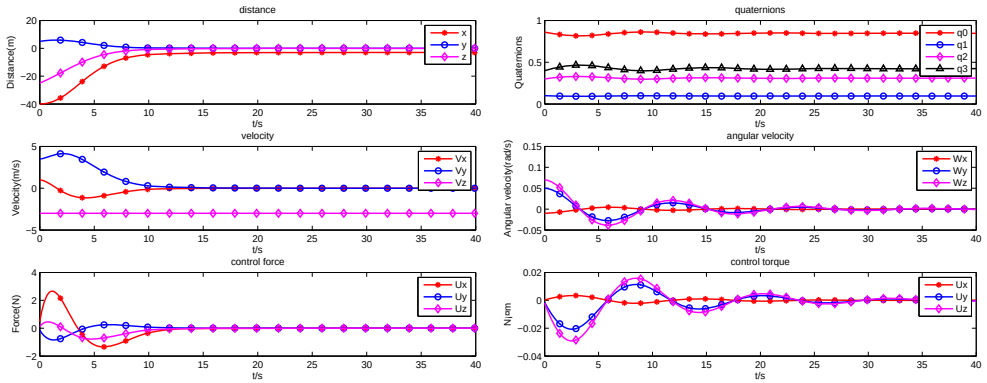

Figure 10. Relative motion states of Sat 1

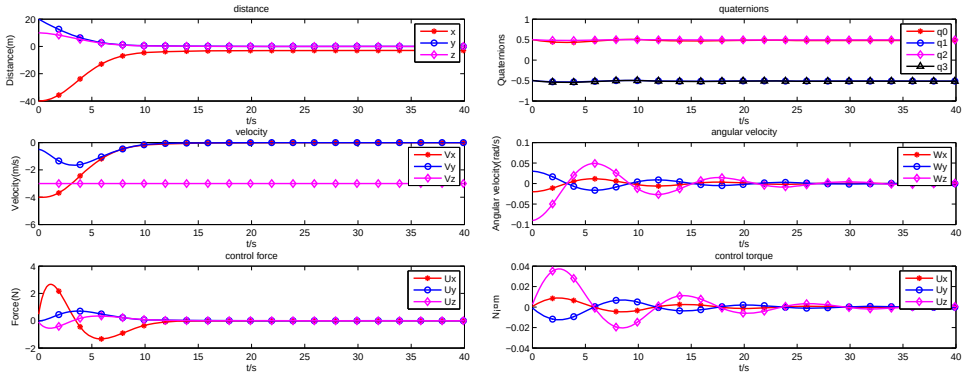

Figure 11. Relative motion states of Sat 2

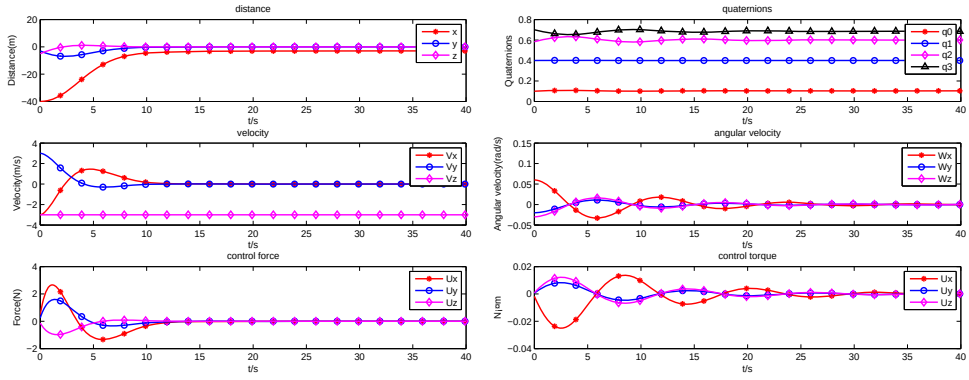

Figure 12. Relative motion states of Sat 3

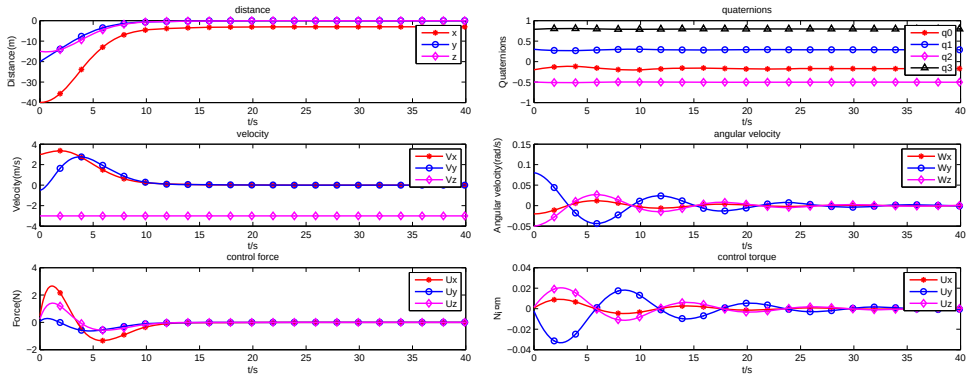

Figure 13. Relative motion states of Sat 4

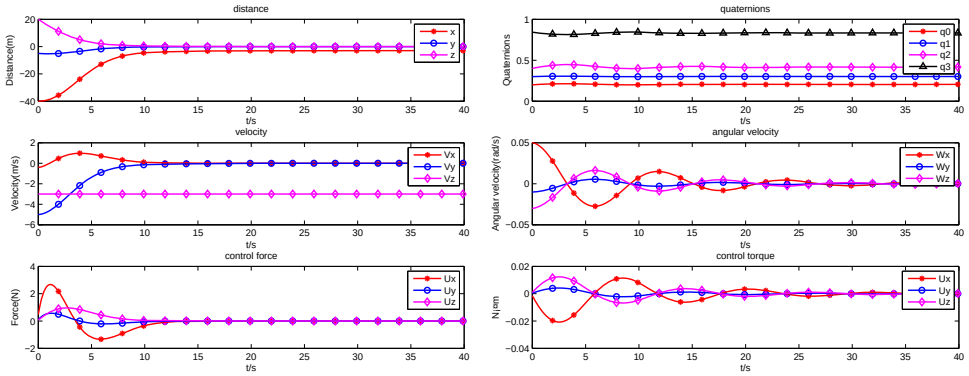

Figure 14. Relative motion states of Sat 5

4.2 Tumbling Target

The height of the target satellite is $800km$, and the corresponding orbital rate is $n = 0.001rad/s$, and the total simulation time is 35 seconds. Through multiple simulations, the control horizon and prediction horizon are $N_c = 20$ and $N = 55$ respectively. The weighting matrices were chosen to be: $\boldsymbol{Q} = 0.01 \times I_{N \cdot state\_num}$, $\boldsymbol{R} = 50 \times I_{N_c \cdot ctrl\_num}$ .The target is tumbling at a speed of $\omega_p = 0.01rad/s$, and the initial relative position and velocity are $[-20, 0, 35]^{\mathrm{T}}\ m$ and $[0.5, 0.3, -0.5]^{\mathrm{T}}\ m/s$. The target and chaser spacecraft masses are 800.0 and 400.0 Kg respectively. Note that the target's states are observed or estimated from measurements carried out by the chaser.

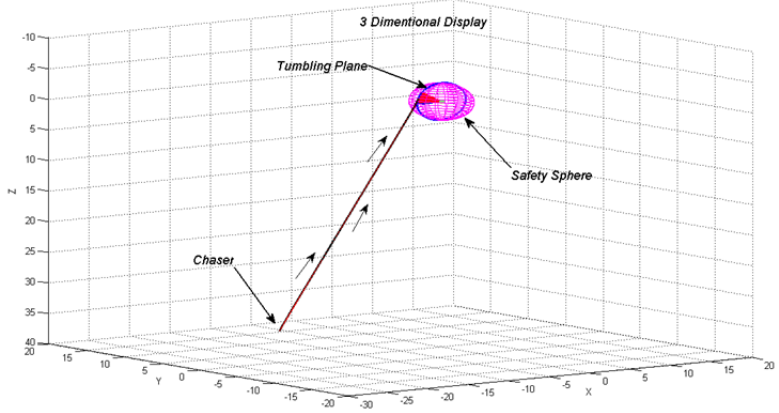

Figure 15. Approaching a tumbling target

As can be seen from the pictures, the quaternions track the time-varying values closely and the angular velocity converges to the ideal angular velocity within less than 10 seconds. Meanwhile, the control torque is moderate and can be satisfied by the current reaction wheels or small-output thrusters.

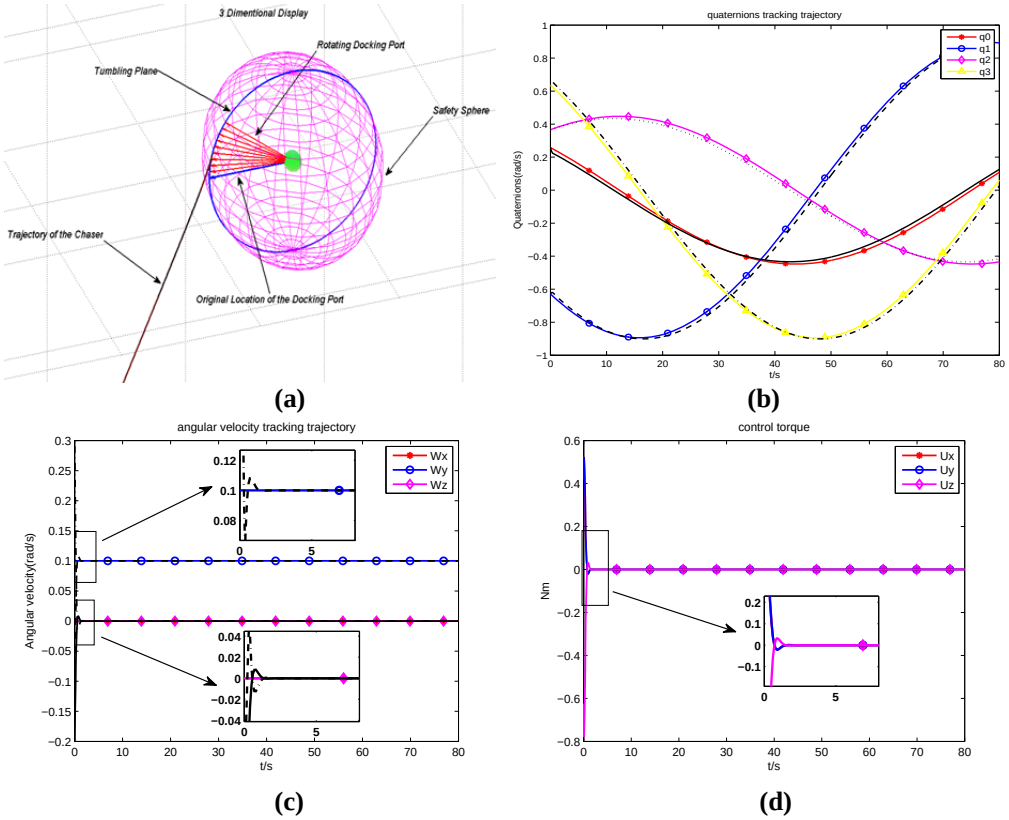

Figure 16. (a) Magnification of figure 15; (b) quaternions; (c) angular velocity; (d) control torque

5 Conclusion

The paper presents a 26-state model of a two-spacecraft rendezvous. The optimal control problems are formulated and addressed using the SDMPC control methods. Both scenarios of approaching a three-axis attitude stabilized target and a tumbling target are considered and the simulations are implemented. Moreover, the solutions obtained are verified numerically by using Matlab. The results obtained show the good performance of the SDMPC. It is also found that path constraints are necessary when solving for the optimal trajectory in order to prevent undesired collision of the spacecraft.

6 Acknowledgements

The authors wish to thank gratefully National Key Laboratory of Aerospace Flight Dynamics in Northwestern Polytechnical University, Xi'an, China, for their support. This work is supported by the National Natural Science Foundation of China (11172235) and Innovation Foundation of Shanghai Aerospace Science and Technology.

7 References

[1] Hablani, H. B., Tapper, M. L., and Dana-Bashian, D. J., “Guidance and Relative Navigation for Autonomous Rendezvous in a Circular Orbit,” Journal of Guidance, Control and Dynamics, Vol. 25, No 3, 2002, pp. 553-562.

[2] Lembeck, C. A., and Prussing, J. E., “Optimal Impulsive Intercept with Low-Thrust Rendezvous Return,” Journal of Guidance, Control, and Dynamics, Vol. 16, No. 3, 1993, pp. 426–433. doi:10.2514/3.21027.

[3] Guelman, M., and Aleshin, M., “Optimal Bounded Low-Thrust Rendezvous with Fixed Terminal-Approach Direction,” Journal of Guidance, Control, and Dynamics, Vol. 24, No. 2, 2001, pp. 378–385. doi:10.2514/2.4722.

[4] Richards, A., Schouwenaars, T., How, J. P., and Feron, E., “Spacecraft Trajectory Planning with Avoidance Constraints Using Mixed-Integer Linear Programming,” Journal of Guidance, Control, and Dynamics, Vol. 25, No. 4, 2002, pp. 755–764. doi:10.2514/2.4943

[5] Breger, L., and How, J. P., “Safe Trajectories for Autonomous Rendezvous of Spacecraft” , Journal of Guidance, Control, and Dynamics, Vol. 31, No. 5, 2008, pp. 1478–1489.

[6] Benson, D. A., Gauss pseudospectral transcription for optimal control [D]. Cambridge: Department of Aeronautics and Astronautics, Massachusetts Institute of Technology, 2004.

[7] Huntington G. T. Advancement and analysis of a Gauss pseudospectral transcription for optimal control problems [D]. Cambridge: Department of Aeronautics and Astronautics, MIT, 2007

[8] Boyarko, G., Yakimenko, O., and Romano, M., “Optimal Rendezvous Trajectories of a Controlled Spacecraft and a Tumbling Object” , Journal of Guidance, Control and Dynamics, Vol. 34, No 4, 2011, pp. 1239-1252.

[9] Lopez, I., and Mclnnes, C. R., “Autonomous Rendezvous Using Artificial Potential Function Guidance”, Journal of Guidance, Control and Dynamics, Vol. 18, No. 4, 1995, pp. 237-241.

[10] Mclnnes, C. R., Autonomous path planning for on-orbit servicing vehicles [J]. Journal of the British Interplanetary Society, 2000, 53: 26 - 38.

[11] Ender S. J., Mclnnes, C. R., and Finn A., “Safety–Critical Autonomous Spacecraft Proximity Operations via Potential Function Guidance” [C]. , 45th AIAA Aerospace Sciences Meeting and Exhibit, Reno, Nevada, Jan. 8-11, 2007.

[12] Richard Epenoy, Fuel optimization for continuous thrust orbital rendezvous with collision avoidance constraint [J], Journal of Guidance, Control and Dynamics, Vol. 34, No. 2, 2011, pp. 493–503.

[13] Louis Breger, Jonathan P. How, Gauss’s Variational Equation-Based Dynamics and Control for Formation Flying Spacecraft [J], Journal of Guidance, Control and Dynamics, Vol. 30, No. 2, 2007, pp. 437–448.

[14] Edward N. Hartley, Model predictive control system design and implementation for spacecraft rendezvous. Control Engineering Practice, Vol. 20, No. 7, 2012, pp. 695–713.

[15] Gavilan, F., Vazquez, R., Chance-constrained model predictive control for spacecraft rendezvous with disturbance estimation. Control Engineering Practice, Vol. 20, No. 2, 2012, pp. 111–122.